

# Synthetic-to-Real Self-supervised Robust Depth Estimation via Learning with Motion and Structure Priors

Weilong Yan<sup>1</sup> Ming Li<sup>3</sup> Haipeng Li<sup>4</sup> Shuwei Shao<sup>5</sup> Robby T. Tan<sup>1,2</sup>

<sup>1</sup>National University of Singapore

<sup>2</sup>ASUS Intelligent Cloud Services

<sup>3</sup>Guangdong Laboratory of Artificial Intelligence and Digital Economy (SZ)

<sup>4</sup>University of Electronic Science and Technology of China

<sup>5</sup>School of Control Science and Engineering, Shandong University

yanweilong@u.nus.edu

## Abstract

*Self-supervised depth estimation from monocular cameras in diverse outdoor conditions, such as daytime, rain, and nighttime, is challenging due to the difficulty of learning universal representations and the severe lack of labeled real-world adverse data. Previous methods either rely on synthetic inputs and pseudo-depth labels or directly apply daytime strategies to adverse conditions, resulting in sub-optimal results. In this paper, we present the first synthetic-to-real robust depth estimation framework, incorporating motion and structure priors to capture real-world knowledge effectively. In the synthetic adaptation, we transfer motion-structure knowledge inside cost volumes for better robust representation, using a frozen daytime model to train a depth estimator in synthetic adverse conditions. In the innovative real adaptation, which targets to fix synthetic-real gaps, models trained earlier identify the weather-insensitive regions with a designed consistency-reweighting strategy to emphasize valid pseudo-labels. We introduce a new regularization by gathering explicit depth distribution to constrain the model facing real-world data. Experiments show that our method outperforms the state-of-the-art across diverse conditions in multi-frame and single-frame evaluations. We achieve improvements of 7.5% and 4.3% in AbsRel and RMSE on average for nuScenes and Robotcar datasets (daytime, nighttime, rain). In zero-shot evaluation of DrivingStereo (rain, fog), our method generalizes better than previous ones. The code is at [Syn2Real-Depth](#).*

## 1. Introduction

Depth estimation from monocular cameras is a fundamental task in computer vision, essential for applications such as autonomous driving, robotics, and closely connected with segmentation [40]. Due to the high cost and difficulty

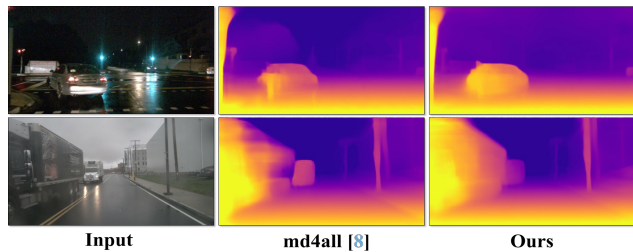


Figure 1. Visual comparison between the previous [8] and ours. The first and second rows correspond to nighttime and rain, where ours provides more robust estimations especially for the vehicles.

of obtaining reliable ground truth, self-supervised methods focusing on photometric and geometric consistency [4, 10, 20, 31, 32, 39, 42, 48] have been developed to reduce dependence on expensive hardware. Early self-supervised methods perform depth inference on single images [10, 48], while recent multi-frame methods [3, 6, 12, 33, 34] for monocular videos achieve improved accuracy. However, these methods generally assume daytime conditions, limiting their generalizability to various adverse scenarios.

Predicting depth in adverse conditions within a single model faces two major challenges: (1) the diverse types of degradation make it difficult to learn a unified representation; (2) the lack of labeled real data makes it difficult to learn in adverse conditions in the real world. To overcome these challenges, many methods are designed for depth estimation in adverse conditions within an unsupervised domain adaptive (UDA) manner [8, 22, 25, 28, 29]. They aim to adapt knowledge from daytime to different adverse conditions and can be divided into single-condition and multi-condition categories. Single-condition methods [23, 26, 30, 44] focus on a particular case (e.g., nighttime) with specific designs, but are quite limited to work under multiple conditions in real-world applications. Some methods [18, 27] aim to address both daytime and nighttime conditions but exhibit limited performance across these do-

mains, often failing to generalize to multiple conditions.

Recently, several approaches [8, 22, 25, 28, 29] have emerged to develop a single model that performs well across diverse conditions. These methods either explore data augmentation and generation techniques [21, 35, 38, 45, 49] to create paired data and employ teacher-student training, or apply photometric loss directly to adverse conditions, alongside a generative adversarial network (GAN) to discriminate the style of predicted depth. While these approaches have advanced the community, they still face challenges in learning robustness facing real-world degradation. On one hand, solely learning from depth pseudo-labels is insufficient for robust common representation due to the heterogeneous nature of different conditions [29, 47]. On the other hand, applying GANs or photometric loss to real adverse data either imposes implicit constraints with sampling randomness or violates the brightness consistency assumption [8, 22]. Furthermore, relying only on synthetic data risks overfitting to the synthetic domain, which still faces the out-of-distribution issue. These motivate us to explore an auxiliary space for improved representation learning and an effective strategy to learn in real-world conditions.

In this work, we propose the first synthetic-to-real framework to achieve depth estimation under diverse conditions. Different from previous methods focused solely on synthetic data, ours learns from the synthetic to real-world data. Since only pseudo-depth label is insufficient for the model to learn due to the heterogeneous features [29, 47], we dig into motion constraint and explicit structure prior for efficient learning of real-world knowledge. Examples of our method compared with previous ones are shown in Fig.1. Starting from having a strong self-supervised daytime model, we identify the cost volume [6, 33, 34] as an effective auxiliary space for robust representation, as it naturally filters redundant information while preserving motion and structural features. Thus, in the synthetic adaptation (SA) which learns on the synthetic data, we construct cost volumes from high-level features to transfer filtered daytime motion-spatial knowledge to adverse conditions, apart from learning only with pseudo-depth labels.

To address the synthetic-real gaps, we propose a novel real adaptation (RA) stage. One challenge is to find valid supervision signals from earlier trained models, and we design a consistency-reweighting strategy by incorporating different models to find a consistency map that can emphasize the valid parts of pseudo-labels and provide effective signals for learning in real-world conditions. Since pseudo-labels from the frozen model still suffer from the synthetic-real gap, we introduce an effective prior based on daytime depth predictions, by calculating explicit depth distribution from the daytime model and setting it to be a reference in diverse conditions. This structural prior provides explicit constraint when facing real adverse data, learning real-world

information further effectively.

With the proposed synthetic-to-real adaptation pipeline, our model can provide much more robust depth predictions in diverse conditions through different real-world datasets [5, 19, 37]. Our contributions are listed as follows:

- We propose a novel synthetic-to-real adaptation pipeline for robust depth estimation in diverse conditions, which is able to work in multiple real-world datasets.
- We construct the motion and cost volume as auxiliary space to transfer filtered daytime knowledge for depth, which boosts the robust representation learning.
- We design a novel real adaptation with two strategies named consistency-reweighting and structure prior constraint, which effectively learns from real adverse data.
- Through the experiments, our method achieves state-of-the-art performance on multiple real challenging datasets (improving by 7.5% in AbsRel and 4.3% in RMSE), in multi-frame, single-frame, zero-shot settings.

## 2. Related Work

### 2.1. Self-supervised Depth Estimation

In the deep learning era [14–17, 43], self-supervised depth has been widely studied for its reliance on only RGB data. SfM-Learner [48] firstly leveraged photometric consistency to reformulate depth estimation as a view reconstruction task. Monodepth2 [10] introduced per-pixel photometric loss and auto-masking to reduce the impact of moving objects. SC-DepthV1 [4] and V3 [24] aimed to address depth scale ambiguity and high dynamic scenes, respectively. MonoViT [42] combines CNN and Transformer capabilities, while Lite-mono [39] offers a lightweight approach. These single-frame methods inspired multi-frame designs, such as Manydepth [33], which utilizes cost volumes across consecutive frames to improve accuracy. DepthFormer [12] introduced an attention mechanism for refining cost volumes, DualRefine [3] iteratively updates depth and pose, while DynamicDepth [6] and Prodepth [34] tackle dynamic object challenges. Though effective in daytime, these methods typically struggle in adverse conditions.

### 2.2. Robust Depth Estimation

Early approaches are tailored to specific conditions. ADFA [26] and RNW [30] use GANs to distinguish features and depth maps in nighttime conditions, while ITDFA [41] employs GANs to translate daytime images to nighttime. STEPS [44] and RNW [30] focus on image enhancement to aid depth estimation. However, these methods, with some works [18, 23, 27] addressing daytime and nighttime, are limited in real-world applications of multiple conditions.

Recent methods [8, 22, 25, 28, 29] target multiple conditions, using data augmentation and generation techniques such as GANs and diffusion models [21, 38, 45, 49] to cre-

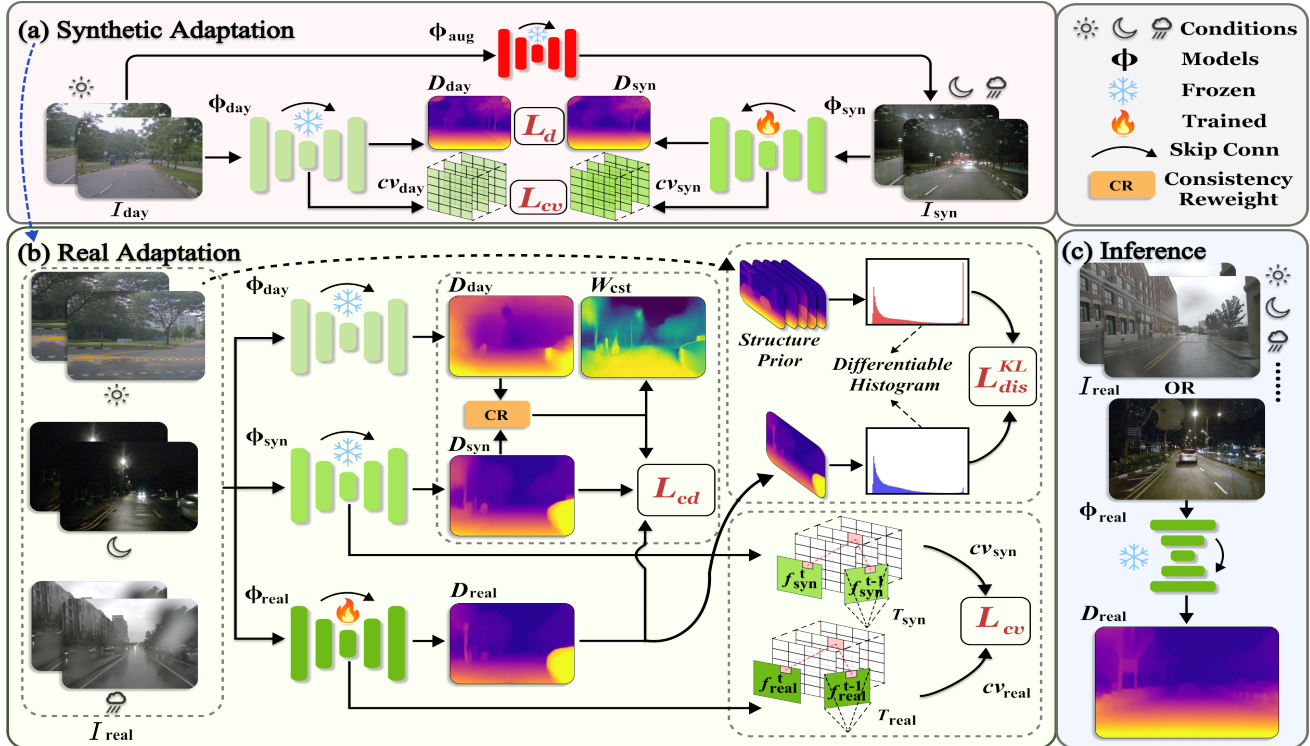


Figure 2. Illustration of our proposed pipeline. (a) Synthetic adaptation utilizes an augmentation model to generate paired data for training, and we also conduct learning in an auxiliary motion space. (b) Real adaptation leverages the daytime model and synthetic model to provide valid pseudo-labels with consistency reweighting, and the daytime depth distribution from plenty of daytime predictions are seen as structure prior to constrain the model facing real adverse data. (c) Inference stage can work in multi-frame and single-frame settings.

ate realistic adverse data and employing a teacher-student framework. However, they overlook the importance of learning a common representation and do not consider about bridging the synthetic-real gap. In contrast, we propose an auxiliary space to enhance robust representation learning and introduce a novel real adaptation stage.

### 3. Proposed Method

We propose to estimate depth map from single frame or consecutive frames under various conditions, including the normal (e.g., daytime) and adverse scenarios (e.g., rain, nighttime, etc.). We demonstrate our pipeline in Fig. 2, which consists of a) Synthetic Adaptation (SA); b) Real Adaptation (RA). In SA, we train a network on synthetic data where: 1) daytime images are fed into a pre-trained daytime model to produce the pseudo depth label; 2) clean images are passed by an augmentation process to synthesise adverse images which are used to train a network to estimate depth maps, supervised by pseudo labels. We discuss the technique details in Sec. 3.1 and Sec. 3.2. To further learn the ability to handle real-world adverse images, we design a novel synthetic-to-real process by importing the motion structure priors, pseudo label reweighting strategy as discussed in Sec. 3.3. Due to limited space, we omit the

symbol for the pose network in Fig. 2.

#### 3.1. Preliminaries

Robust depth estimation is closely connected with self-supervised depth estimation since it can provide a good daytime model for the adaptation. For the good performance as well as the motion-structure information in daytime, we choose Manydepth [33] as our daytime baseline and implement on nuScenes and Robotcar datasets [5, 19] with all daytime data.

The pipeline of Manydepth [33] consists of a depth network  $\Phi_{D-day}$  and a pose network  $\Phi_{P-day}$ , the key of which is to inject multi-frame cost volume  $cv$  into the model to give explicit geometric guidance. The input of the models are consecutive frame pairs  $I_{t-1}, I_t$ , and the cost volume  $cv$  is constructed via  $I_{t-1}, I_t$  and the encoder of  $\Phi_{D-day}$ :

$$cv = \Phi_{D-day}(I_t) - W(\Phi_{D-day}(I_{t-1}), T, d, K), \quad (1)$$

$$T = \Phi_{P-day}(I_t, I_{t-1}), \quad (2)$$

where  $W(\cdot)$  is the warping operation [36],  $T$  represents the estimated pose,  $d$  is the predefined depth candidates and  $K$  refers to the camera intrinsics. In short, the depth  $D_t$  is obtained by

$$D_t = \Phi_{D-day}(I_t, cv). \quad (3)$$

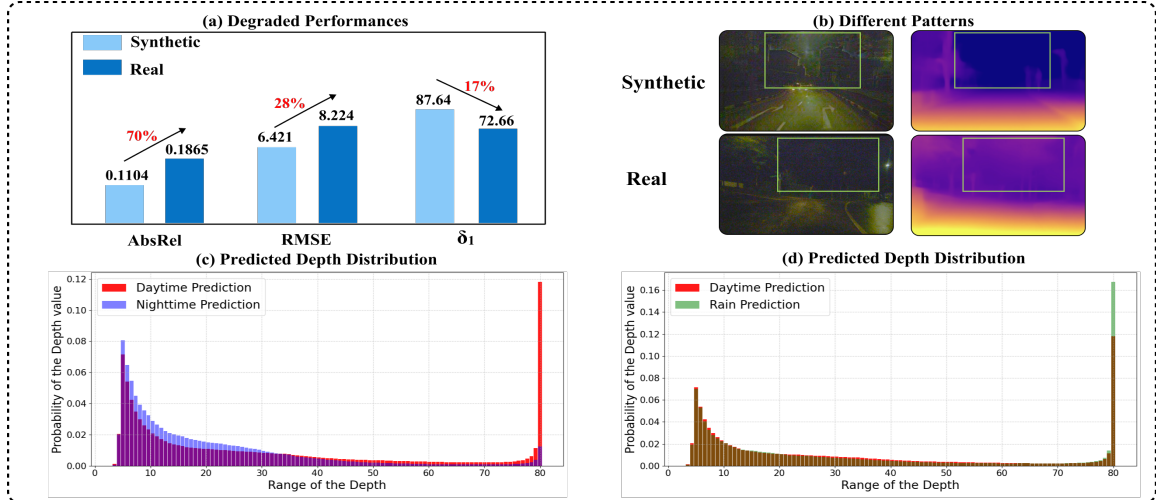


Figure 3. Analysis on our design. (a) Illustration of the gaps between the synthetic and real data on performance. (b) Green boxes emphasize the different pattern between synthetic and real data, which affects the model’s estimation especially for far planes. (c)-(d) The distribution difference between the daytime predicted depth and estimated depth in adverse conditions.

In the training, it also requires a single-frame model as a reference to provide the consistent map  $M$  and guidance to the inconsistent parts. The total objective function is

$$L = (1 - M)L_p + L_{consist} + L_{smooth}, \quad (4)$$

where  $L_p$  and  $L_{smooth}$  are the typical losses for self-supervised depth [9, 10, 48].  $L_{consist}$  is a constraint from the single-frame model. Training on monocular videos provides a strong model to work in normal conditions but suffer from degradation cases, and that’s why adapting to both normal and adverse conditions is important.

### 3.2. Synthetic Adaptation with Motion and CV

Since we do not have real daytime-adverse paired data, directly adapting a daytime model to multiple adverse conditions is difficult. Following [8, 22, 25, 28], we first adapt the pre-trained daytime models  $\Phi_{D-day}$ ,  $\Phi_{P-day}$  (denoted as  $\Phi_{day}$  in Fig.2) to synthetic adverse model  $\Phi_{D-syn}$ ,  $\Phi_{P-syn}$ . To realize that, a generative adversarial network (GAN) [45, 49] or a diffusion model [21] defined as  $\Phi_{aug}$  is utilized as augmentations to translate the daytime images into multiple adverse conditions as

$$I_{C_i-syn} = \Phi_{aug}(I_{day}), C_i \in C, \quad (5)$$

where  $C$  represents the set of conditions. Then the adaptation can be conducted on the paired data  $I_{day}, I_{C_i-syn}$  in a distillation or teacher-student manner, where the outputs of  $\Phi_{D-day}, \Phi_{P-day}$  can be defined as  $D_{day}, T_{day}$  and those from  $\Phi_{D-syn}, \Phi_{P-syn}$  are  $D_{syn}, T_{syn}$ . The distillation objective is the absolute relative depth loss:

$$L_d = \frac{1}{HW} \sum \left| \frac{D_{day} - D_{syn}}{D_{syn}} \right|. \quad (6)$$

However, learning from only depth pseudo labels is still challenging to learn about the adverse patterns [29, 46], which motivates us to also discover an auxiliary space to inhibit the problems. Surprisingly, we find that the cost volume can be an auxiliary space to transfer the knowledge. In theory, the process of constructing cost volume is naturally filtering out the abundant information, which retains explicit motion and structure information and reflects the pixel-level correlation through temporal frames. This gives us chances to distill explicit and filtered motion and structure knowledge from daytime to adverse conditions.

The cost volumes from  $\Phi_{D-day}$  and  $\Phi_{D-syn}$  are defined as  $cv_{day}, cv_{syn}$ . Thus, the objective of cost volume learning is added into training:

$$L_{cv} = \frac{1}{chw} \sum |cv_{day} - cv_{syn}|. \quad (7)$$

To construct the correct cost volume, we also supervise the  $T_{syn}$  by  $T_{day}$  with an L2 loss  $L_T$ . The synthetic adaptation is illustrated in Fig.2 (a), where the total objective  $L_{syn}$  is designed with different scale factors:

$$L_{syn} = \alpha_1 L_d + \alpha_2 L_{cv} + \alpha_3 L_T. \quad (8)$$

We also notice that the cost volume constructed by feature dot product can lead to more robust learning compared with feature difference. Thus Eq.1 will be changed into  $cv = \Phi_{D-day}(I_t) \cdot W(\Phi_{D-day}(I_{t-1}), T, d, K)$ .

### 3.3. Real Adaptation with Consistency Reweighting and Structure Prior

Although synthetic adaptation helps to bridge the gap between daytime and synthetic adverse conditions, there are

still inevitable gaps between synthetic and real adverse conditions [8, 22, 46]. Here, we analyze the performance of models  $\Phi_{D-syn}$  and  $\Phi_{P-syn}$  on synthetic and real data under the same condition (e.g., night), as shown in Fig.3 (a) and (b). In (a), performance significantly declines from synthetic to real adverse data, with drops of 70% in *AbsRel*, 28% in *RMSE*, and 17% in  $\delta_1$ . In (b), the synthetic nighttime image and its predicted depth map show different patterns compared to the real nighttime, such as successful detection of near and far distances in synthetic images, and failure to detect distant planes in real images. This motivates us to address the synthetic-real domain gap.

Formally, our goal is to train a depth model  $\Phi_{D-real}$  and a pose model  $\Phi_{P-real}$  capable of predicting  $D_{real}$  across various real conditions without any labels. To achieve this, we leverage the abilities of  $\Phi_{D-day}$  and  $\Phi_{D-syn}$  by carefully designing a Real Adaptation stage in Fig. 3 (b).

**Consistency Reweighting Strategy** A straightforward supervision signal for  $D_{real}$  is  $D_{syn}$ , generated by  $\Phi_{D-syn}$  on real data, which can serve as a pseudo label for  $\Phi_{D-real}$ . However, since  $\Phi_{D-syn}$  is optimized for the synthetic domain and may not perform well in real adverse conditions, it is intuitive to emphasize supervision on the more reliable parts. To address this, we also leverage  $\Phi_{D-day}$  to provide predictions  $D_{day}$  on real images across diverse conditions. Our strategy compares  $D_{day}$  and  $D_{syn}$ , assigning higher weights to consistent regions and lower weights to highly inconsistent areas. Using an exponential function [34], we design a confidence map  $C_{cst}$  based on the consistency and transform it into a reweighting map  $W_{cst}$ :

$$C_{cst} = e^{-\beta \frac{|D_{syn} - D_{day}|}{D_{syn}}}, \quad (9)$$

$$W_{cst} = C_{cst} + \epsilon. \quad (10)$$

The  $\beta$  is a scale factor and the  $\epsilon$  is a weight bias to guarantee a weak supervision. The supervision for  $D_{real}$  will be changed into a reweighting consistent-depth loss  $L_{cd}$ :

$$L_{cd} = \frac{1}{HW} \sum W_{cst} \left| \frac{D_{real} - D_{syn}}{D_{real}} \right|. \quad (11)$$

**Structure Prior Constraint** Although pseudo-label learning is reweighted, it still cannot perfectly supervise real adverse predictions, motivating us to seek more explicit priors from daytime data and depth. To investigate further, we calculate and visualize the predicted depth distributions of  $\Phi_{D-day}$  and  $\Phi_{D-syn}$  on the real training set in Fig.3 (c) and (d). In (c), we observe that the primary distribution difference between nighttime and daytime is at the far planes (e.g., near 80, the model’s upper prediction limit). Notably, nighttime depth contains more near-plane predictions ( $< 30$ ) compared to daytime depth, consistent with poor visibility at long distances under nighttime conditions,

causing the model to predict more areas as closer. In contrast, Fig.3 (d) shows that under rainy condition, the model predicts more distant regions, likely due to rain-induced blur misleading the model to perceive near objects as farther away.

Inspired by these insights, we set the daytime predicted distribution as a reference and aim to align the distributions of adverse conditions with that of daytime. Formally, the distributions for daytime and adverse conditions are defined as  $Dist_{day}$  and  $Dist_{adv}$ , obtained from the predicted depth values across defined depth bins. However, direct calculation of these distributions makes the histogram indifferentiable. Following [1, 2], we use differentiable histograms to capture these distributions. We define  $N$  sub-intervals between  $d_{min}$  and  $d_{max}$ , where each interval has a length of  $L = \frac{d_{max} - d_{min}}{N}$ , with center  $b_n = d_{min} + L(n + \frac{1}{2})$  for interval  $n$ . Using two sigmoid functions  $\sigma$  to model the kernel function  $K(x) = \sigma(x)\sigma(-x)$ , the probability of a depth map  $D$  falling within interval  $k$  is

$$P(n) = \frac{1}{HW} \sum_{x=1}^{HW} \left[ \sigma\left(\frac{D(x) - b_n + \frac{L}{2}}{a}\right) - \sigma\left(\frac{D(x) - b_n - \frac{L}{2}}{a}\right) \right], \quad (12)$$

where  $P$  is the differentiable probability function and  $a$  is a bandwidth factor. Finally, the  $Dist_{day}$ ,  $Dist_{adv}$  are consist of  $P_{day}$ ,  $P_{adv}$ :

$$Dist_{day} = \{b_n, P_{day}(n)\}_{n=1}^N, \quad (13)$$

$$Dist_{adv} = \{b_n, P_{adv}(n)\}_{n=1}^N. \quad (14)$$

Noted that  $Dist_{day}$  is calculated among the whole daytime training set instead of one sample. The objective is to minimize the distribution distances between  $Dist_{day}$  and  $Dist_{adv}$  by K-L divergence:

$$L_{dis}^{KL} = \sum_{i=1}^N P_{adv}(i) \cdot \log \frac{P_{adv}(i)}{P_{day}(i)}. \quad (15)$$

Apart from  $L_{cd}$  and  $L_{dis}^{KL}$ , we also utilize  $L_{cv}$  and  $L_T$  as in previous stage. Thus, the total objective function  $L_{real}$  is

$$L_{real} = \alpha_1 L_{cd} + \alpha_2 L_{dis}^{KL} + \alpha_3 L_{cv} + \alpha_4 L_T \quad (16)$$

With the designed learning procedure, our model can gradually fit better to multiple real conditions, rather than only learn from the synthetic conditions.

## 4. Experiments

### 4.1. Implementation Details

The experiments on all models of different stages are conducted on the same ResNet architecture [13], so do the baselines. The training for the  $\Phi_{day}$  and the  $\Phi_{syn}$  are conducted for 20 epochs, while  $\Phi_{real}$  is initialized by  $\Phi_{syn}$

Method	Test frames	nuScenes-day				nuScenes-night				nuScenes-rain			
		AbsRel↓	SqRel↓	RMSE↓	$\delta_1$ ↑	AbsRel↓	SqRel↓	RMSE↓	$\delta_1$ ↑	AbsRel↓	SqRel↓	RMSE↓	$\delta_1$ ↑
Monodepth2 [10]	1	0.1333	1.820	6.459	<u>85.88</u>	0.2419	2.776	10.922	58.17	0.1572	2.273	7.453	79.49
R4Dyn <sup>†</sup> (Radar) [7]	1	<u>0.1259</u>	<u>1.661</u>	<u>6.434</u>	<b>86.97</b>	0.2194	2.889	10.542	62.28	<u>0.1337</u>	1.938	7.131	<b>83.91</b>
RNW [30]	1	0.2872	3.433	9.185	56.21	0.3333	4.066	10.098	43.72	0.2952	3.796	9.341	57.21
md4all-AD [8]	1	0.1523	2.141	6.853	83.11	0.2187	2.991	9.003	68.84	0.1601	2.259	7.832	78.97
robust-depth [22]	1	0.1436	1.862	6.802	82.95	0.2101	2.691	8.673	69.58	0.1458	1.891	7.371	80.21
md4all-DD [8]	1	0.1366	1.752	6.452	84.61	0.1921	<u>2.386</u>	8.507	71.07	0.1414	<u>1.829</u>	7.228	80.98
DM-MDE [25]	1	0.1280	-	6.449	84.03	<u>0.1910</u>	-	<u>8.433</u>	<b>71.14</b>	0.1390	-	<u>7.129</u>	<u>81.36</u>
<b>Ours-Single</b>	1	<b>0.1239</b>	<b>1.454</b>	<b>6.214</b>	85.66	<b>0.1792</b>	<b>1.896</b>	<b>7.949</b>	<u>71.08</u>	<b>0.1331</b>	<b>1.616</b>	<b>6.926</b>	<b>81.68</b>
Manydepth [33]	2(-1,0)	0.1213	1.699	6.183	<b>87.05</b>	0.2442	3.347	11.38	57.04	0.1347	1.730	7.110	81.24
Manydepth [33]+[8]	2(-1,0)	0.1202	1.417	6.111	86.62	0.1865	2.255	8.245	72.58	0.1310	1.717	6.840	82.61
<b>Ours-Multi</b>	2(-1,0)	<b>0.1170</b>	<b>1.371</b>	<b>6.023</b>	86.66	<b>0.1713</b>	<b>1.779</b>	<b>7.689</b>	<b>73.16</b>	<b>0.1266</b>	<b>1.532</b>	<b>6.654</b>	<b>82.86</b>

Table 1. Quantitative comparison on nuScenes in different conditions (daytime, nighttime and rain). <sup>†</sup> indicates the method [7] using **additional Radar information**. Test frames indicates the evaluation is conducted in multi-frame or single-frame setting. - points to the missing value from the reference. The first and second ranked performances are indicated by **bold** and underline.

Method	Source	Test frames	Robotcar-day				Robotcar-night			
			AbsRel↓	SqRel↓	RMSE↓	$\delta_1$ ↑	AbsRel↓	SqRel↓	RMSE↓	$\delta_1$ ↑
Monodepth2 [10]	[8]	1	0.1209	0.723	3.335	86.61	0.3909	3.547	8.227	22.51
DeFeatNet [23]	[27]	1	0.2470	2.980	7.884	65.00	0.3340	4.589	8.606	58.60
ADIDS [18]	[27]	1	0.2390	2.089	6.743	61.40	0.2870	2.569	7.985	49.00
RNW [30]	[27]	1	0.2970	2.608	7.996	43.10	0.1850	1.710	6.549	73.30
WSGD [27]	[27]	1	0.1760	1.603	6.036	75.00	0.1740	1.637	6.302	75.40
robust-depth [22]	[self]	1	0.1225	0.776	3.302	85.84	0.1333	0.895	3.756	85.11
md4all [8]	[8]	1	0.1128	<u>0.648</u>	<u>3.206</u>	87.13	<u>0.1219</u>	0.784	<u>3.604</u>	84.86
DM-MDE [25]	[25]	1	0.1190	0.728	3.287	87.17	0.1290	<u>0.751</u>	3.661	83.86
Manydepth [33]	[self]	1	0.1200	0.802	3.413	87.46	0.4974	5.517	10.21	14.87
Manydepth [33]+[8]	[self]	1	<u>0.1092</u>	0.759	3.355	<b>88.32</b>	0.1257	0.930	3.904	<u>85.24</u>
<b>Ours-Single</b>	[self]	1	<b>0.1063</b>	<b>0.646</b>	<b>3.171</b>	<u>88.29</u>	<b>0.1103</b>	<b>0.693</b>	<b>3.455</b>	<b>86.15</b>

Table 2. Quantitative comparison on Robotcar dataset [19] in different conditions (daytime and nighttime). Source indicates where the metrics are cited, and [self] refers to our own implementations.

Method	Test frames	DrivingStereo-rain			
		AbsRel↓	SqRel↓	RMSE↓	$\delta_1$ ↑
robust-depth [22]	1	0.2622	4.309	11.657	59.58
md4all [8]	1	0.1822	2.007	8.465	70.35
Manydepth [33]+[8]	1	0.1852	2.020	8.515	69.24
<b>Ours-Single</b>	1	<b>0.1707</b>	<b>1.755</b>	<b>8.004</b>	<b>72.98</b>
Method	Test frames	DrivingStereo-fog			
		AbsRel↓	SqRel↓	RMSE↓	$\delta_1$ ↑
robust-depth [22]	1	0.1366	1.260	6.876	84.01
md4all [8]	1	<b>0.1259</b>	1.081	<b>6.383</b>	<b>86.16</b>
Manydepth [33]+[8]	1	0.1335	1.162	6.740	83.50
<b>Ours-Single</b>	1	0.1281	<b>1.023</b>	6.422	84.52

Table 3. Zero-shot evaluation on DrivingStereo (rain, fog). Noted that our method is designed for both single-frame and multi-frame settings, and definitely defeats the compared baseline [33]+[8].

and trained for 10 epochs. The learning rate is initialized to  $1 \times 10^{-4}$  with a decreasing factor of 0.5 every 5 epochs. For the adaptive depth bins in Manydepth [33], we fix them to  $3.5 - 80m$  since [8, 11, 25] all use a weak velocity loss

to align the scales. Thanks to [8, 25], we can utilize the synthetic data from their pretrained augmentation models. For the  $Dist_{day}$ , we obtain a fixed distribution through the whole daytime training dataset, and utilize it for the real adaptation constraint. Similar to [8, 22], our training is conducted with a mixture of daytime and adverse data, and more details can be found in the supplementary.

## 4.2. Datasets

Our approach is evaluated on three mainstream public datasets for robust depth estimation, including nuScenes [5] and Robotcar [19] which are used for training and testing, and DrivingStereo [37] dataset which is used for zero-shot evaluation to verify the effectiveness of our pipeline.

**NuScenes** [5] is a large benchmark which owns real data in daytime, nighttime, and rain conditions with 15 hours of driving. Following [7, 8, 25], a total of 21476 images (including 15129 in daytime, 3796 in rain, 2551 in nighttime) are considered for training. For evaluation, the set owns 6019 consecutive frame pairs (4449 in daytime, 1088

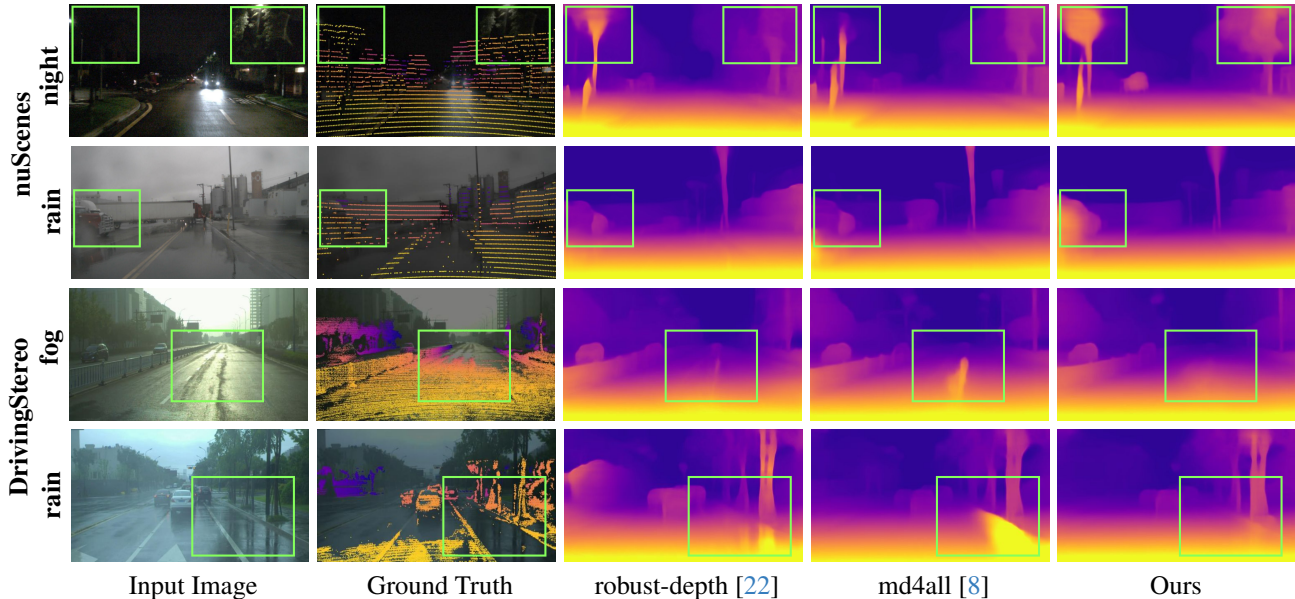


Figure 4. Qualitative comparison of depth predictions under adverse conditions. The first two rows refer to nighttime and rain conditions in nuScenes [5] dataset, and the last two rows are zero-shot evaluation results on DrivingStereo [37] dataset. Our method addresses the challenging cases indicated in green boxes (can be checked via the ground truth), where other methods fail.

in rain, 602 in nighttime). Our model is evaluated both under single-frame and multi-frames settings. All the metrics are computed for ground truth within  $0.1 - 80m$ .

**Robotcar** [19] contains daytime and nighttime driving data. We follow the split of WSGD [27], where there are 17790 images in daytime and 19612 in nighttime. The test set includes 1411 single images, in which 702 are daytime and 709 are nighttime. Our model is evaluated in single-frame setting on the dataset, with the depth range of  $0.1 - 50m$ .

**DrivingStereo** [37] is a dataset that includes the real rainy and foggy images, where each condition includes 500 single images for our zero-shot evaluation. We follow the use of data in [28] to evaluate our model in single-frame setting and all metrics are computed within a range of  $0.1 - 80m$ .

### 4.3. Evaluation Metrics and Baselines

Following previous methods [8, 10, 25, 33], we set the absolute relative error (AbsRel), square relative error (SqRel), root mean square error (RMSE), and threshold accuracy ( $\delta_1$ ) as the evaluation protocol. We choose the competitive state-of-the-art methods as our baselines, including [8, 22, 25, 27, 30] with their baseline [10], the Radar-based method [7], and [18, 23]. Since our multi-frame training pipeline is built on [33], we also compare with [33] and a self-designed baseline [33]+[8] (using only synthetic adverse data with pseudo labels to train Manydepth).

### 4.4. Quantitative Experimental Results

Our quantitative results across different datasets are shown in Tables 1-3. Tab. 1 presents evaluations on the nuScenes

dataset [5] under various conditions (daytime, nighttime, rain) in single-frame (two inputs of the model are the same frame) and multi-frame settings (two inputs are consecutive frames), where our method significantly outperforms prior approaches. Specifically, in the single-frame setting, we achieve average improvements of 4.8%, 16.8%, 4.2% on AbsRel, SqRel, and RMSE, respectively, over recent methods [8, 25] that rely on synthetic data, highlighting the impact of real data for robustness. In the multi-frame setting, our method also surpasses the baseline [33]+[8], and even surpasses radar-based methods [7]. Tab. 2 shows results on the Robotcar dataset [19] across daytime and nighttime domains. Since the test set contains only single-frame samples, we compare our method in the single-frame setting, achieving average improvements of 7.8%, 6.5%, 2.7% on AbsRel, SqRel, and RMSE against recent methods [8, 25]. Notably, the baseline [33]+[8] can not outperform previous single-frame methods. However, the model trained from our pipeline achieves noticeable improvements. **This indicates that the performance is not gained from the multi-frame backbone but from our training strategy.**

We also evaluate different methods on the DrivingStereo dataset [37] (rain, fog) in a zero-shot setting, conducting in single-frame mode due to the lack of consecutive frames, as illustrated in Tab. 3. Ours surpasses the state-of-the-art by 3.0%, 10.0%, 2.8% on AbsRel, SqRel, and RMSE, demonstrating stronger generalization ability over models trained on only synthetic data. Notably, our model significantly outperforms the fairly-designed baseline [33]+[8] in both rain and fog conditions.

Modules						nuScenes-night				nuScenes-rain			
SA	$L_{feat}$	$L_{cv}$	RA	CR	$L_{dis}^{KL}$	AbsRel↓	SqRel↓	RMSE↓	$\delta 1 \uparrow$	AbsRel↓	SqRel↓	RMSE↓	$\delta 1 \uparrow$
✓						0.1865	2.255	8.245	72.58	0.1310	1.717	6.840	82.61
✓	✓					0.1911	2.495	8.456	72.41	0.1335	1.756	7.056	82.04
✓		✓				0.1809	2.019	7.988	72.61	0.1290	1.657	6.794	82.76
✓		✓	✓			0.1781	1.892	7.896	72.45	0.1288	1.610	6.856	82.36
✓		✓	✓	✓		0.1743	1.809	7.716	73.10	0.1256	1.576	6.743	82.82
✓		✓	✓	✓	✓	<b>0.1713</b>	<b>1.779</b>	<b>7.689</b>	<b>73.16</b>	<b>0.1266</b>	<b>1.532</b>	<b>6.654</b>	<b>82.86</b>

Table 4. Ablations on each module and stage mentioned in the pipeline. The checkmark represents utility of the corresponding module. SA refers to the synthetic adaptation with only depth supervision, and RA is training on real data with only pseudo label in real adaptation.

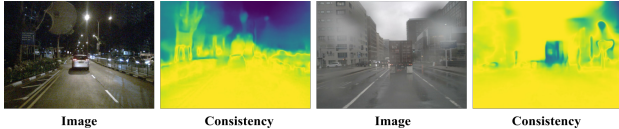


Figure 5. Visualization of consistency maps.

#### 4.5. Qualitative Experimental Results

Our qualitative results across various adverse conditions are shown in Fig.4. Due to space constraints, we display results from nuScenes and DrivingStereo; additional examples are provided in the supplementary materials. Since [25] is not open source, we compare with the latest methods [8, 22].

Rows 1 and 2 show nuScenes examples under night and rain conditions. In row 1, the dark regions obscure details, yet the ground truth reveals a road sign on the left and trees on the right (highlighted in green). Robust-depth [22] and md4all [8] struggle in these areas, missing the road sign and misestimating the depth of the trees. In contrast, our model provides reasonable depth predictions, closely aligning with the ground truth. Row 2 illustrates a rainy scene with a blurry region partially obscuring a car. This blur causes [8, 22] to overestimate depth, consistent with Fig.3 (d). Our model, however, accurately identifies the nearby car, producing depth values close to the ground truth. Row 3 shows a foggy scene from DrivingStereo, where previous methods misinterpret tire trails on the road as obstacles, while our model correctly ignores them, generating a smooth depth map. Row 4 presents a rainy DrivingStereo scene where reflections challenge even LiDAR depth capture, as shown in the green box. Both [8, 22] are affected by reflections, but our model remains robust, providing depth consistent with geometric features. These examples demonstrate our model’s adaptability to diverse real-world conditions.

#### 4.6. Analysis on Consistency Reweighting

Examples of consistency maps discussed in Sec.3.3 are shown in Fig.5, where brighter areas indicate higher consistency. The first two columns correspond to night conditions, showing that dark, distant regions exhibit low consistency between  $D_{day}$  and  $D_{syn}$ , while near regions have much stronger consistency. The last two columns represent

rain conditions, where the blurry areas show low consistency. This allows us to select the more reliable regions. More visualization results can be seen in supplementary.

### 5. Ablations

To verify the effectiveness of each stage and the designed modules, we conduct ablations on learning from the cost volume ( $L_{cv}$ ), real adaptation without designed strategies (RA), consistency reweighting (CR), and structure prior constraint ( $L_{dis}^{KL}$ ). Additionally, we compare learning from the cost volume with direct learning from daytime features ( $L_{feat}$ ). The baseline is trained solely with depth loss in the synthetic adaptation (SA). Due to space limitations, we provide results for night and rain conditions in Tab.4.

Given the abundant information within features and the heterogeneous visual cues across conditions, simply using  $L_{feat}$  leads to significantly worse performance than the baseline. In contrast, since the cost volume inherently filters extraneous information and retains motion-structure features, utilizing  $L_{cv}$  enhances the model’s performance in adverse scenarios. Moreover, applying RA alone without additional strategies does not guarantee improved performance on real data, as not all supervisions are valid. However, by incorporating  $L_{cv}$  to emphasize valid regions and  $L_{dis}^{KL}$  for structural prior constraint, the model’s performance gradually improves in real-world adverse conditions. The ablation study confirms the effectiveness of the individual components within the pipeline and highlights the importance of synthetic-to-real adaptation.

### 6. Conclusion

In this work, we propose a synthetic-to-real learning pipeline for self-supervised robust depth estimation, including synthetic adaptation and real adaptation stages where the cost volume is constructed to transfer motion-structure feature from daytime to adverse conditions. We introduce a consistency reweighting strategy and a structure prior constraint to boost learning from synthetic to real domains. Experiments across diverse settings and datasets show that our model provides more accurate and robust depth than previous methods, with superior generalization capabilities.

## References

- [1] Mor Avi-Aharon, Assaf Arbelle, and Tammy Riklin Raviv. Hue-net: Intensity-based image-to-image translation with differentiable histogram loss functions. *arXiv preprint arXiv:1912.06044*, 2019. 5
- [2] Mor Avi-Aharon, Assaf Arbelle, and Tammy Riklin Raviv. Differentiable histogram loss functions for intensity-based image-to-image translation. *IEEE Transactions on Pattern Analysis and Machine Intelligence*, pages 1–12, 2023. 5
- [3] Antyanta Bangunharcana, Ahmed Magd Aly, and KyungSoo Kim. Dualrefine: Self-supervised depth and pose estimation through iterative epipolar sampling and refinement toward equilibrium. In *Proceedings of the IEEE/CVF Conference on Computer Vision and Pattern Recognition (CVPR)*. IEEE, 2023. 1, 2
- [4] Jia-Wang Bian, Huangying Zhan, Naiyan Wang, Zhichao Li, Le Zhang, Chunhua Shen, Ming-Ming Cheng, and Ian Reid. Unsupervised scale-consistent depth learning from video. *International Journal of Computer Vision (IJCV)*, 2021. 1, 2
- [5] Holger Caesar, Varun Bankiti, Alex H. Lang, Sourabh Vora, Venice Erin Liong, Qiang Xu, Anush Krishnan, Yu Pan, Giancarlo Baldan, and Oscar Beijbom. nuscenes: A multimodal dataset for autonomous driving. *arXiv preprint arXiv:1903.11027*, 2019. 2, 3, 6, 7
- [6] Ziyue Feng, Liang Yang, Longlong Jing, Haiyan Wang, YingLi Tian, and Bing Li. Disentangling object motion and occlusion for unsupervised multi-frame monocular depth. *arXiv preprint arXiv:2203.15174*, 2022. 1, 2
- [7] Stefano Gasperini, Patrick Koch, Vinzenz Dallabetta, Nassir Navab, Benjamin Busam, and Federico Tombari. R4dyn: Exploring radar for self-supervised monocular depth estimation of dynamic scenes. In *2021 International Conference on 3D Vision (3DV)*, pages 751–760. IEEE, 2021. 6, 7
- [8] Stefano Gasperini, Nils Morbitzer, HyunJun Jung, Nassir Navab, and Federico Tombari. Robust monocular depth estimation under challenging conditions. In *Proceedings of the IEEE/CVF International Conference on Computer Vision*, pages 8177–8186, 2023. 1, 2, 4, 5, 6, 7, 8
- [9] Clément Godard, Oisín Mac Aodha, and Gabriel J. Brostow. Unsupervised monocular depth estimation with left-right consistency. In *2017 IEEE Conference on Computer Vision and Pattern Recognition (CVPR)*, pages 6602–6611, 2017. 4
- [10] Clément Godard, Oisín Mac Aodha, Michael Firman, and Gabriel J Brostow. Digging into self-supervised monocular depth estimation. In *Proceedings of the IEEE/CVF international conference on computer vision*, pages 3828–3838, 2019. 1, 2, 4, 6, 7
- [11] Vitor Guizilini, Rares Ambrus, Sudeep Pillai, Allan Raventos, and Adrien Gaidon. 3d packing for self-supervised monocular depth estimation. In *IEEE Conference on Computer Vision and Pattern Recognition (CVPR)*, 2020. 6
- [12] Vitor Guizilini, Rares Ambrus, Dian Chen, Sergey Zakharov, and Adrien Gaidon. Multi-frame self-supervised depth with transformers. In *Proceedings of the IEEE/CVF Conference on Computer Vision and Pattern Recognition (CVPR)*, pages 160–170, 2022. 1, 2
- [13] Kaiming He, Xiangyu Zhang, Shaoqing Ren, and Jian Sun. Deep residual learning for image recognition. In *2016 IEEE Conference on Computer Vision and Pattern Recognition (CVPR)*, pages 770–778, 2016. 5
- [14] Ming Li, Xinming Huang, and Ziming Zhang. Self-supervised geometric features discovery via interpretable attention for vehicle re-identification and beyond. In *Proceedings of the IEEE/CVF International Conference on Computer Vision (ICCV)*, pages 194–204, 2021. 2
- [15] Ming Li, Jun Liu, Ce Zheng, Xinming Huang, and Ziming Zhang. Exploiting multi-view part-wise correlation via an efficient transformer for vehicle re-identification. *IEEE Transactions on Multimedia*, 25:919–929, 2023.
- [16] Ming Li, Xiangyu Xu, Hehe Fan, Pan Zhou, Jun Liu, Jia-Wei Liu, Jiahe Li, Jussi Keppo, Mike Zheng Shou, and Shuicheng Yan. Strprivacy: Spatio-temporal privacy-preserving action recognition. In *Proceedings of the IEEE/CVF International Conference on Computer Vision (ICCV)*, pages 5106–5115, 2023.
- [17] Ming Li, Pan Zhou, Jia-Wei Liu, Jussi Keppo, Min Lin, Shuicheng Yan, and Xiangyu Xu. Instant3d: Instant text-to-3d generation. *arxiv: 2311.08403*, 2023. 2
- [18] Lina Liu, Xibin Song, Mengmeng Wang, Yong Liu, and Liangjun Zhang. Self-supervised monocular depth estimation for all day images using domain separation. In *Proceedings of the IEEE/CVF International Conference on Computer Vision*, pages 12737–12746, 2021. 1, 2, 6, 7
- [19] W. Maddern, G. Pascoe, C. Linegar, and P. Newman. 1 year, 1000 km: The oxford robotcar dataset. *International Journal of Robotics Research*, page 0278364916679498, 2016. 2, 3, 6, 7
- [20] Rui Peng, Ronggang Wang, Yawen Lai, Luyang Tang, and Yangang Cai. Excavating the potential capacity of self-supervised monocular depth estimation. In *Proceedings of the IEEE International Conference on Computer Vision (ICCV)*, 2021. 1
- [21] Robin Rombach, Andreas Blattmann, Dominik Lorenz, Patrick Esser, and Björn Ommer. High-resolution image synthesis with latent diffusion models. In *Proceedings of the IEEE/CVF Conference on Computer Vision and Pattern Recognition (CVPR)*, pages 10684–10695, 2022. 2, 4
- [22] Kieran Saunders, George Vogiatzis, and Luis J. Manso. Self-supervised monocular depth estimation: Let’s talk about the weather. In *Proceedings of the IEEE/CVF International Conference on Computer Vision (ICCV)*, pages 8907–8917, 2023. 1, 2, 4, 5, 6, 7, 8
- [23] Jaime Spencer, Richard Bowden, and Simon Hadfield. Defeat-net: General monocular depth via simultaneous unsupervised representation learning. In *Proceedings of the IEEE/CVF Conference on Computer Vision and Pattern Recognition*, pages 14402–14413, 2020. 1, 2, 6, 7
- [24] Libo Sun, Jia-Wang Bian, Huangying Zhan, Wei Yin, Ian Reid, and Chunhua Shen. Sc-depthv3: Robust self-supervised monocular depth estimation for dynamic scenes. *IEEE Transactions on Pattern Analysis and Machine Intelligence (TPAMI)*, 2023. 2
- [25] Fabio Tosi, Pierluigi Zama Ramirez, and Matteo Poggi. Diffusion models for monocular depth estimation: Overcoming

- challenging conditions. In *European Conference on Computer Vision (ECCV)*, 2024. 1, 2, 4, 6, 7, 8
- [26] Madhu Vankadari, Sourav Garg, Anima Majumder, Swagat Kumar, and Ardhendu Behera. Unsupervised monocular depth estimation for night-time images using adversarial domain feature adaptation. In *Computer Vision—ECCV 2020: 16th European Conference, Glasgow, UK, August 23–28, 2020, Proceedings, Part XXVIII 16*, pages 443–459. Springer, 2020. 1, 2
- [27] Madhu Vankadari, Stuart Golodetz, Sourav Garg, Sangyun Shin, Andrew Markham, and Niki Trigoni. When the sun goes down: Repairing photometric losses for all-day depth estimation. In *Conference on Robot Learning*, pages 1992–2003. PMLR, 2023. 1, 2, 6, 7
- [28] Jiyuan Wang, Chunyu Lin, Lang Nie, Shujun Huang, Yao Zhao, Xing Pan, and Rui Ai. Weatherdepth: Curriculum contrastive learning for self-supervised depth estimation under adverse weather conditions, 2023. 1, 2, 4, 7
- [29] Jiyuan Wang, Lang Nie, Kang Liao, Shuwei Shao, and Yao Zhao. Digging into contrastive learning for robust depth estimation with diffusion models. In *ACM Int. Conf. Multimedia (ACMMM)*, pages 4129–4137, 2024. 1, 2, 4
- [30] Kun Wang, Zhenyu Zhang, Zhiqiang Yan, Xiang Li, Baobei Xu, Jun Li, and Jian Yang. Regularizing nighttime weirdness: Efficient self-supervised monocular depth estimation in the dark. In *Proceedings of the IEEE/CVF International Conference on Computer Vision*, pages 16055–16064, 2021. 1, 2, 6, 7
- [31] Ruoyu Wang, Zehao Yu, and Shenghua Gao. Planedepth: Self-supervised depth estimation via orthogonal planes. In *2023 IEEE/CVF Conference on Computer Vision and Pattern Recognition (CVPR)*, pages 21425–21434, 2023. 1
- [32] Youhong Wang, Yunji Liang, Hao Xu, Shaohui Jiao, and Hongkai Yu. Sqrdepth: Generalizable self-supervised fine-structured monocular depth estimation, 2023. 1
- [33] Jamie Watson, Oisín Mac Aodha, Victor Prisacariu, Gabriel Brostow, and Michael Firman. The temporal opportunist: Self-supervised multi-frame monocular depth. In *Proceedings of the IEEE/CVF Conference on Computer Vision and Pattern Recognition (CVPR)*, pages 1164–1174, 2021. 1, 2, 3, 6, 7
- [34] Sungmin Woo, Wonjoon Lee, Woo Jin Kim, Dogyoon Lee, and Sangyoun Lee. Prodepth: Boosting self-supervised multi-frame monocular depth with probabilistic fusion. *arXiv preprint arXiv:2407.09303*, 2024. 1, 2, 5
- [35] Yihang Wu, Xiao Cao, Kaixin Li, Zitan Chen, Haonan Wang, Lei Meng, and Zhiyong Huang. Towards better text-to-image generation alignment via attention modulation. *ArXiv*, abs/2404.13899, 2024. 2
- [36] Haofei Xu, Jing Zhang, Jianfei Cai, Hamid Rezatofighi, Fisher Yu, Dacheng Tao, and Andreas Geiger. Unifying flow, stereo and depth estimation. *IEEE Transactions on Pattern Analysis and Machine Intelligence*, 2023. 3
- [37] Guorun Yang, Xiao Song, Chaoqin Huang, Zhidong Deng, Jianping Shi, and Bolei Zhou. Drivingstereo: A large-scale dataset for stereo matching in autonomous driving scenarios. In *IEEE Conference on Computer Vision and Pattern Recognition (CVPR)*, 2019. 2, 6, 7
- [38] Lvmin Zhang, Anyi Rao, and Maneesh Agrawala. Adding conditional control to text-to-image diffusion models. In *IEEE International Conference on Computer Vision (ICCV)*, 2023. 2
- [39] Ning Zhang, Francesco Nex, George Vosselman, and Norman Kerle. Lite-mono: A lightweight cnn and transformer architecture for self-supervised monocular depth estimation. In *Proceedings of the IEEE/CVF Conference on Computer Vision and Pattern Recognition (CVPR)*, pages 18537–18546, 2023. 1, 2
- [40] Xin Zhang, Jinheng Xie, Yuan Yuan, Michael Bi Mi, and Robby T Tan. Heap: unsupervised object discovery and localization with contrastive grouping. In *Proceedings of the AAAI Conference on Artificial Intelligence*, pages 7323–7331, 2024. 1
- [41] Chaoqiang Zhao, Yang Tang, and Qiyu Sun. Unsupervised monocular depth estimation in highly complex environments. *IEEE Transactions on Emerging Topics in Computational Intelligence*, 6(5):1237–1246, 2022. 2
- [42] Chaoqiang Zhao, Youmin Zhang, Matteo Poggi, Fabio Tosi, Xianda Guo, Zheng Zhu, Guan Huang, Yang Tang, and Stefano Mattoccia. Monovit: Self-supervised monocular depth estimation with a vision transformer. In *2022 International Conference on 3D Vision (3DV)*, pages 668–678. IEEE, 2022. 1, 2
- [43] Ce Zheng, Yecheng Lyu, Ming Li, and Ziming Zhang. Lodonet: A deep neural network with 2d keypoint matching for 3d lidar odometry estimation. In *Proceedings of the 28th ACM International Conference on Multimedia*, page 2391–2399, New York, NY, USA, 2020. Association for Computing Machinery. 2
- [44] Yupeng Zheng, Chengliang Zhong, Pengfei Li, Huan-ang Gao, Yuhang Zheng, Bu Jin, Ling Wang, Hao Zhao, Guyue Zhou, Qichao Zhang, and Dongbin Zhao. Steps: Joint self-supervised nighttime image enhancement and depth estimation. In *2023 IEEE International Conference on Robotics and Automation (ICRA)*, pages 4916–4923, 2023. 1, 2
- [45] Ziqiang Zheng, Yang Wu, Xinran Han, and Jianbo Shi. Forkgan: Seeing into the rainy night. In *The IEEE European Conference on Computer Vision (ECCV)*, 2020. 2, 4
- [46] Hanyu Zhou, Yi Chang, Wending Yan, and Luxin Yan. Unsupervised cumulative domain adaptation for foggy scene optical flow. In *Proceedings of the IEEE/CVF Conference on Computer Vision and Pattern Recognition*, pages 9569–9578, 2023. 4, 5
- [47] Hanyu Zhou, Yi Chang, Haoyue Liu, YAN WENDING, Yuxing Duan, Zhiwei Shi, and Luxin Yan. Exploring the common appearance-boundary adaptation for nighttime optical flow. In *The Twelfth International Conference on Learning Representations*, 2024. 2
- [48] Tinghui Zhou, Matthew Brown, Noah Snavely, and David G. Lowe. Unsupervised learning of depth and ego-motion from video. In *2017 IEEE Conference on Computer Vision and Pattern Recognition (CVPR)*, pages 6612–6619, 2017. 1, 2, 4
- [49] Jun-Yan Zhu, Taesung Park, Phillip Isola, and Alexei A Efros. Unpaired image-to-image translation using cycle-consistent adversarial networks. In *Computer Vision*

(ICCV), 2017 IEEE International Conference on, 2017. 2,  
4